Kovove Mater. 60 2022 109–120
DOI: 10.31577/km.2022.2.109

Evaluation of welding parameters effects in friction stir welding of AZ31B Mg alloy

Fatmagül Tolun

Department of Motor Vehicles and Transportation Technologies, Balikesir Vocational High School, Balikesir University, 10145 Balikesir, Turkey

Received 26 August 2021, received in revised form 14 April 2022, accepted 29 April 2022

Abstract

The joining of magnesium alloys with conventional fusion welding methods often causes porosity and hot cracking defects. The use of friction stir welding, a solid-state welding technique for joining Mg alloys, solves these problems. In this study, AZ31B Mg sheets with 3 mm in thickness were joined by friction stir welding at a constant feed rate (50 mm min^{-1}) and different tool rotational speeds (900 and 1400 rpm), and different tool tilt angles (0° and 1.5°) using tapered pin. Tensile strength and microhardness tests were carried out to examine the mechanical properties of the welded specimens. The microstructures of the welded zone were analyzed by obtaining optical microscopy and scanning electron microscopy images. According to the tensile test results, specimen welded at 50 mm min^{-1} feed rate, 900 rpm tool rotational speed, and 1.5° tool tilt angle showed the highest welding strength value 176.03 MPa.

K e y w o r d s: friction stir welding, magnesium alloys, welding parameters, microstructure, tensile strength

1. Introduction

Magnesium alloys display properties of low density, high strength/weight ratio, good thermal conductivity, excellent damping capacity, good castability, good machinability, and reusability. These properties of Mg alloys are the nominee to displace aluminum in automobile and aerospace applications. Using Mg alloys in automobile and aerospace applications reduces fuel consumption and emission gas output [1–3]. The welding of Mg alloys with conventional fusion welding methods generally causes defects such as porosity and hot cracking. These defects decline the mechanical properties of welded joints. Friction stir welding (FSW), a solid-state welding technique, was developed and patented by the Welding Institute in the United Kingdom in 1991. The use of FSW to join Mg alloys solves these problems [4–6].

When the previous studies are examined, it is seen that Mg alloys were joined by different welding methods such as diffusion welding [7], laser welding [8], laser-arc hybrid welding [9], gas tungsten arc welding [10], laser-tungsten inert gas arc welding [11], metal inert gas welding [12], electron beam welding [13]. FSW has high weld strength values, smooth welding surfaces, no need for additional materials such as electrodes, fillers, powder and shielding gas, no emissions, no radiation, shortening of welding time, low energy consumption, low cost, and automation compatibility is one of the most advantageous welding methods in joining Mg alloys. FSW is an environmentally friendly welding technology [14, 15].

M. Sucharitha et al. [16] studied material flow behavior and mechanical properties of dissimilar FSWed Al 7075 and Mg AZ31 alloys using Cd interlayer. They observed the supersaturated solid solution of Mg in Al, a thin layer of Al_3Mg_2, and small particles of $Al_{12}Mg_{17}$ in the stir zone (SZ). They determined that the formation of intermetallic compounds (IMCs) could be prevented because Cd reacted with Mg only and formed CdMg and CdMg3 compounds distributed in Mg alloy as lamellar-like structures and provided micromechanical interlocking. They found out the flow behavior of the cadmium interlayer controls the formation of brittle $Al_{12}Mg_{17}$ IMCs in the nugget zone (NZ). Ankit Thakur et al. [17] investigated the effect of tool tilt

*Corresponding author: e-mail address: ftolun@balikesir.edu.tr

angle on weld joint strength and microstructural characterization of double-sided FSWing of AZ31B magnesium alloy. Joint W1 and Joint W2 were welded by FSW at tool rotational speed of 800 rpm and 50 mm/min feed rate. In the study, two tool tilt angles of 0° (Joint W1) and 2° (Joint W2) were used. Welding results demonstrated tunnel defect in joint W1 and defect-free joint in W2.

The dissimilar AM60/AZ31 Mg alloys joints were obtained via FSW and were examined by Junlei Zhang et al. [18]. The dissimilar AM60/AZ31 Mg alloys were jointed by FSW. Then, the upper and lower surfaces of the welded joints were remelted with tungsten inert gas (TIG) welding. According to the study results, there was a TIG weld zone in both the upper and lower parts of the NZ of the FSW joint after the arc heating. Also, the grain size in the NZ-middle grew to a certain extent, especially in the area near the NZ--middle-center. M. Sucharitha et al. [19] studied the effect of tool rotational speed on mechanical properties and microstructure of FSWed AZ31 Mg alloy. A threaded cylindrical tool was used for the FSW process. Results indicated that high tensile strength was obtained for a joint welded at a tool rotational speed of 1120 rpm, whereas high hardness was found at a tool rotational speed of 900 rpm. Furthermore, at a tool rotational speed of 1120 rpm, grain size reduction occurred.

The microstructural and tensile properties of AZ31B Mg alloy joints by stationary shoulder FSW were investigated by Wenya Li et al. [20]. The study showed that a bowl-shaped stir zone (SZ) with fine equiaxed grains is present, and its grain size grows as the tool's rotational speed rises. The lowest Vickers hardness occurred in the thermo-mechanically affected zone (TMAZ) on the advancing side (AS). When the tool rotational speed rose, the ultimate tensile strength of joints also rose, while the yield stress and elongation at fracture decreased. P. Kumar et al. [21] studied the microstructure and mechanical behavior of FSWed AZ91-D magnesium alloy. Optimization of process parameters was used by the Taguchi method. According to the results, the optimum levels of process parameters were tool rotational speed of 1000 rpm, feed rate of 50 mm min^{-1}, and the number of passes was 6. Additionally, microhardness tests were performed to approve the process optimization. The welded specimens with optimized parameters showed an enhancement of 24.56 and 77.5 % in ultimate tensile strength and microhardness compared to the base material.

Nan Xu et al. [22] examined the mechanical properties' modification of large load FSWed AZ31B Mg alloy joint. In the study, large load FSW associated with a very low feed rate and tool rotational speed rate was applied to an AZ31B Mg alloy to modify the microstructure, the texture, and the mechanical properties of the joint. It was seen that the twin structure in the weld provided adequate barriers for dislocation motion for strengthening and created more local sites for nucleating and accommodating dislocations, thereby elevating ductility and strain hardening of the weld. Also, the work provided a basic and efficient method to increase the strength of an FSW Mg joint without ductility loss. The tensile behavior of FSWed AZ31 Mg alloy was investigated by S. Mironov et al. [23]. Results of the study demonstrated that the feature of measured strain patterns indicated the prevalence of basal slip and suggested significant prism slip activity. A substantial strain gradient was found lengthways in the SZ. The failure was shown to be initiated at the weld root and to originate from double twinning. The crack propagation was affected by the onion-ring structure of the SZ.

Hui Shi et al. [24] examined the IMCs in the banded structure (BS) and their effect on mechanical properties of Al/Mg dissimilar FSW joints. They found large quantities of IMCs in the form of alternating bands of particles or lamellae in the BS zone, where severe material intermixing occurred during FSW. The results showed that tool rotational speed affected the morphology of the microstructure of the BS and the distribution of IMCs particles. All of the welded joints displayed fracture mode with their fracture paths generating along the IMCs in the BS.

AZ31B Mg alloy has a wide range of applications such as aircraft fuselage, automobile constructional parts, components, and machine tool parts undergoing rapid acceleration and retardation [25]. The welding of AZ31B Mg alloy and other Mg alloys with conventional fusion welding methods causes unwanted defects such as porosity and hot cracking. But FSW can solve these defects. From the prior literature overview, it can be seen that the relationship welding parameters for welding of Mg alloys by FSW need to be studied further. Thus this study focuses on joining AZ31B Mg alloy through FSW, and the effects of welding parameters such as tool rotational speed and tool tilt angle on microstructure and mechanical properties of welded joints are investigated.

2. Experimental procedure

2.1. Materials and welding procedure

In this study, AZ31B Mg sheets with dimensions of 3 mm × 100 mm × 150 mm were used. The nominal chemical compositions and mechanical properties of AZ31B Mg alloy were determined by Varzene Metal Industry and Trade Inc. and are introduced in Table 1.

A tapered pin tool was used in the study. It was made of 1.3343 high-speed steel and had a hardness of 62 HRC by using heat treatment, and its shoulder

Table 1. The nominal chemical compositions and mechanical properties of AZ31B Mg alloy

Materials	Nominal chemical composition (wt.%)							Mechanical properties		
	Al	Mg	Si	Mn	Fe	Cu	Zn	Yield strength (MPa)	Tensile strength (MPa)	Hardness ($HV_{0.1}$)
AZ31B Mg	3.05	Bal	0.015	0.2	0.001	0.003	0.7	166	229	62

Table 2. The variations of welding parameters

Parameter number	Feed rate (mm min^{-1})	Tool rotational speed (rpm)	Tool tilt angle
1	50	900	0°
2	50	1400	0°
3	50	900	1.5°
4	50	1400	1.5°

diameter was 12 mm, pin depth 2.95 mm, the outer diameter of the tapered pin 3 mm, and inner diameter 1.5 mm.

The variations of welding parameters determined regarding preliminary studies in the experiment are presented in Table 2. FSW processes were performed with a constant feed rate of 50 mm min^{-1}, different tool rotational speeds of 900 and 1400 rpm, and different tool tilt angles of 0° and 1.5°. Before welding, to remove the oxide layer and other contaminants, all surfaces of the Mg sheets were sanded with SiC sandpaper and then wiped with pure alcohol. AZ31B Mg sheets were joined with butt welding with a welding direction perpendicularly to the rolling direction through the FSW method. Figure 1a shows the FSW process of AZ31B Mg sheets. In the coding of the welding parameters, the values of the feed rate, tool tilt angle, and tool rotational speed were used (50/0°/900), respectively.

Universal milling machine (Taksan FU 315 × 1250) was used for the welding process. In the joining process, the waiting time at the start of welding was taken as 30 s and the tool rotated in a clockwise direction.

2.2. Measurement of mechanical properties

After the FSW process, welded specimens performed the tensile tests. Specimens were drawn by using Zwick Roel tensile tester. Three specimens with a weld seam in the middle and following the ASTM E08 M-04 standard [26] were prepared for all welding parameters. The drawing speed of the tensile test was determined 2 mm min^{-1} at all the tensile tests, and the tensile strengths of specimens were measured perpendicular to the welding direction. Figure 1b presents images of tensile test specimens.

The hardness values of the specimens joined through FSW were measured on the Vickers scale

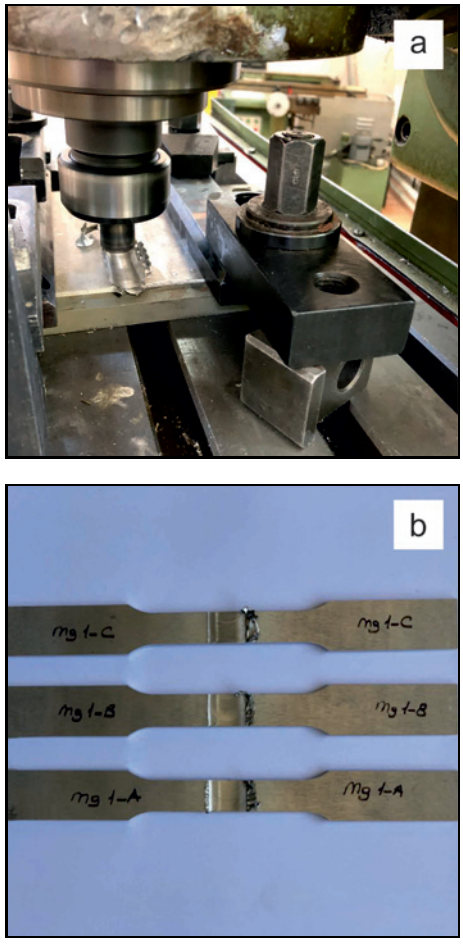

Fig. 1. Images of (a) FSW process of AZ31B Mg sheets and (b) tensile test specimens.

($HV_{0.1}$). Shimadzu HMV microhardness tester was used in the measurements. Measurement was performed for every 1 mm along a line perpendicular to

Fig. 2. Surface images of (a) Specimen 1, (b) Specimen 2, (c) Specimen 3, and (d) Specimen 4.

the welding seam direction on the welding surface, and a 100 g load was applied for a dwell period of 15 s in the microhardness test.

2.3. Microstructure characterization

For the microscopic examinations, firstly, specimens with a cross-section perpendicular to the welding direction were inserted in the bakelite mold. Secondly, the weld cross-section of specimens was sanded with sandpaper of 220 to 1200 grit, and they were polished with 3 μm and 1 μm diamond paste. In the last step, specimens were etched for 12 s with Picral reagent, which was obtained by mixing 10 ml acetic acid, 10 ml distilled water, 6 g picric acid, and 100 ml ethanol. In addition, 10 nm gold plating was applied to the samples to realize the scanning electron microscope (SEM) imaging of the welded zone.

After the FSW process, the microstructure changes of specimens were observed under an optical microscope (OM) (Nikon DS-Fi1) and SEM (FEI QUANTA 250 FEG). Energy-dispersive X-ray spectroscopy (EDX) analyses were performed to determine the localized chemical composition of the welding zone.

3. Results and discussion

In this study, AZ31B Mg alloy was successfully joined by FSW. Results of FSW of AZ31B Mg alloy are given below. Figures 2a–d show the surface images of the specimens welded through FSW. Figure 2a presents Specimen 1 (50/0°/900), Fig. 2b presents Specimen 2 (50/0°/1400), Fig. 2c presents Specimen 3 (50/1.5°/900), and Fig. 2d presents Specimen 4 (50/1.5°/1400). Figure 2 demonstrates that the weld seams of Specimens 1, 3, and 4 are smooth and even, while those of Specimen 2 are rough and uneven. Specimen 2 showed the lowest welding strength according to the tensile test results. Therefore, the rough and uneven structure observed in the welding seam of Specimen 2 is thought to negatively affect the mechanical properties of the welding region [4, 14].

Figure 3 shows the results of the tensile tests of the welded specimens. Specimen 3 (50/1.5°/900) demonstrated the highest value of welding strength (176.03 MPa). Its welding performance was 76.86 %, corresponding to the base metal (BM).

The value of the welding strength of Specimen 4 (50/1.5°/1400) was 162.94 MPa. The value of the

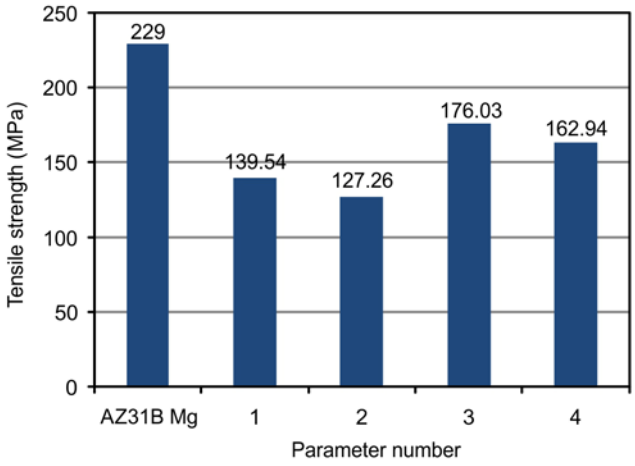

Fig. 3. Results of the tensile tests of the welded specimens.

welding strength of Specimen 4 was lower than that of Specimen 3. Specimens 3 and 4 were joined under the same tool tilt angle but at different rotational speeds. When the tool rotational speed was increased from 900 to 1400 rpm, welding strength was decreased. Tool rotational speed affects the intensity of plastic deformation occurring in the weld zone during the welding, affecting material mixing. High tool rotation speed with the unnecessary release of stirred material on the top surface leads to defects, such as poor surface (flash), voids, porosity, tunneling, or wormhole formation, due to the extremely high heat input generated by welding [4, 14, 27–28]. During the joining of AZ31B Mg alloy by FSW, $Al_{12}Mg_{17}$ IMCs occur. The IMCs have a needle shape and lead to the loss of strength. Because the $Al_{12}Mg_{17}$ IMCs peaked at a high tool rotational speed of 1400 rpm, the welding strength of the specimens welding under a tool rotational speed of 1400 rpm was decreased [4, 6, 17, 19].

The welding strength of Specimen 1 (50/0°/900) was 139.54 MPa. This value was lower than the values of Specimens 3 and 4. When the tool tilt angle was lacking in the welding process, the welding strength decreased. Specimen 2 (50/0°/1400) showed the lowest welding strength (127.26 MPa) in the study. The welding performance of Specimen 2 was 55.57 %, corresponding to the BM. The welding of Specimen 2 was performed under a tool tilt angle of 0° and a tool rotational speed of 1400 rpm. Because of this, the welding strength of Specimen 2 was the lowest value in the study. According to previous studies, when the FSW process was performed under tool tilt angles, welded specimens showed good mechanical properties [4, 6, 14, 29]. The study results demonstrated that the tool tilt angle also had an important effect on the mechanical properties of the welded specimens. The highest strength values of welded specimens were observed in the welding processes when a 1.5° tool tilt angle was used.

Also, microhardness values were measured at the transverse cross-section of Specimens 1, 2, 3, and 4. Figure 4 presents microhardness values of Specimens 1, 2, 3, and 4. All joints showed typical W-shaped microhardness profiles in the welding area. The microhardness measurement graphs indicated that the hardness values of all the specimens were similar. It is seen that the microhardness values were increased in the SZ of specimens. The SZ's grain size is thinner than the AZ31B Mg BM's grain size. A homogeneously distributed fine-grained structure occurred in the SZ region, in which the stirring action occurred in the welding area. The SZ generally shows a structure with grain refinement and strain hardening [1, 14, 17, 22]. As it moves away from the welding center, values

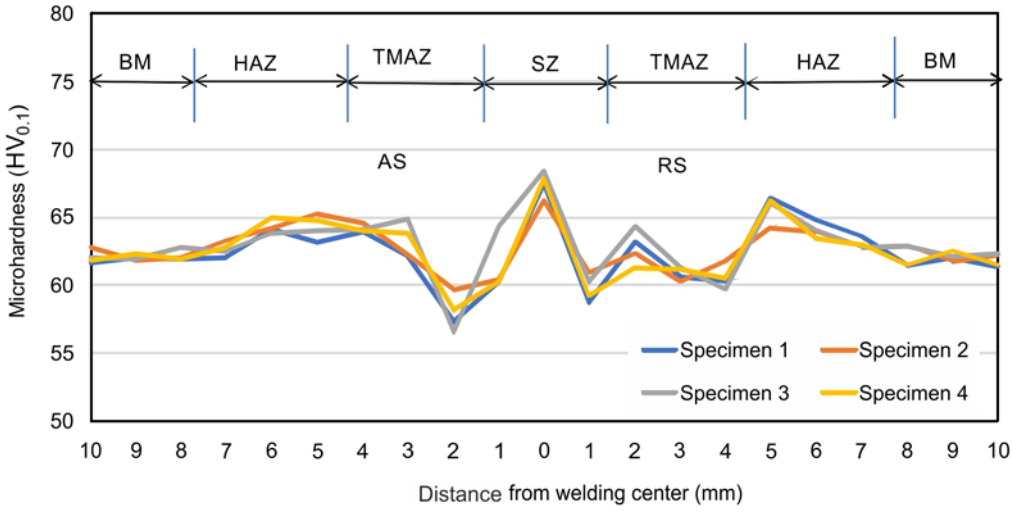

Fig. 4. Microhardness values of Specimens 1, 2, 3, and 4.

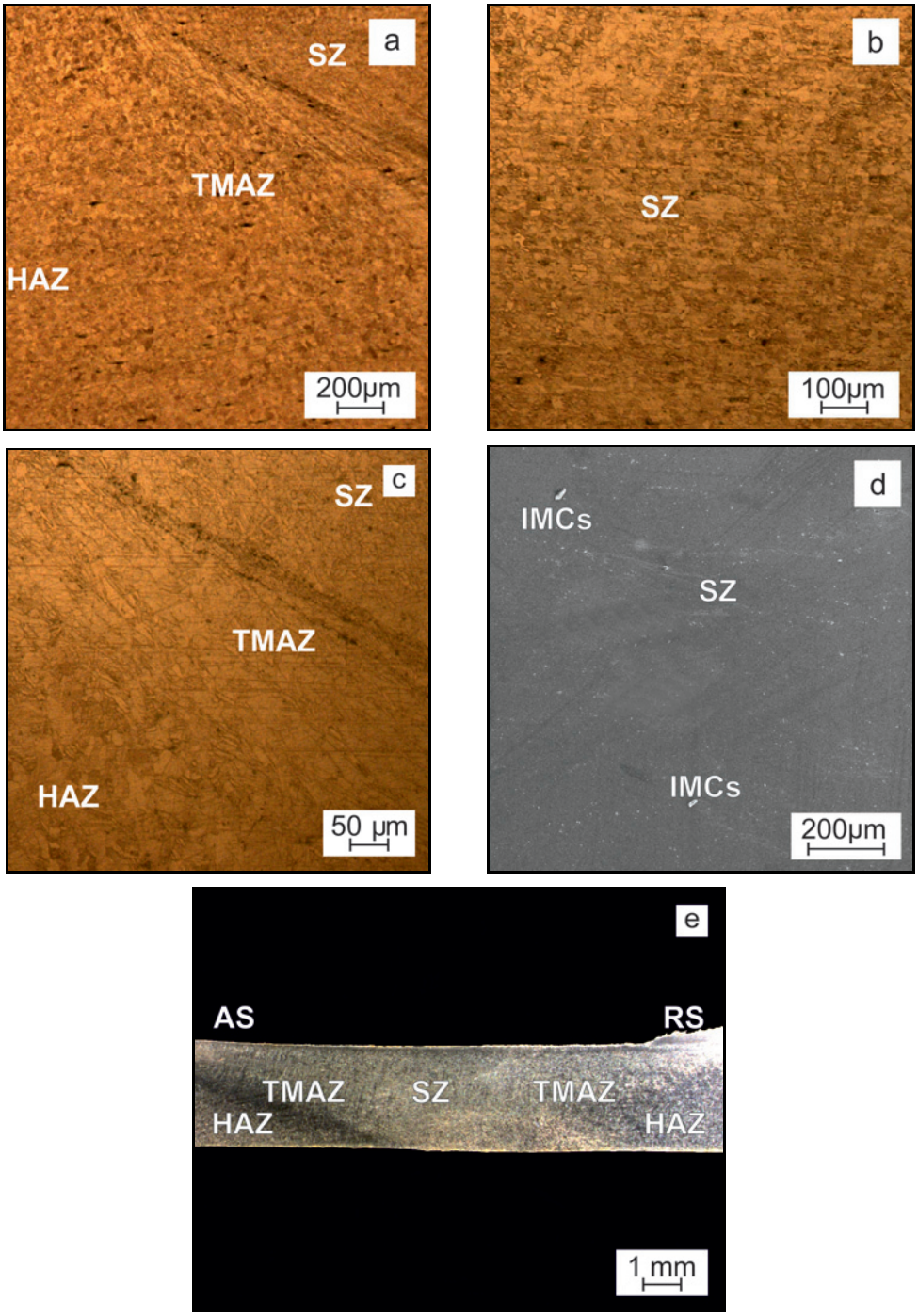

Fig. 5. OM and SEM images of (a) SZ, TMAZ and HAZ regions, (b) SZ region, (c) TMAZ and HAZ regions, (d) IMCs in the SZ zone, and (e) weld region of Specimen 3.

close to the microhardness value of the base material were measured. The microhardness values were decreased in the TMAZ and heat affected zone (HAZ). The hardness decreased in the HAZ and TMAZ due to grain growth in these zones during the FSW [20, 22]. The lowest hardness distribution is in the TMAZ of the AS at all specimens. Previous studies also support this [6, 20]. According to the literature, while the AS displayed a sharp heterogeneous microstructure at the SZ/TMAZ interface, the retreating side (RS) showed a more homogeneous microstructure that underwent a more gradual change [25]. It can be thought that the AS and RS were affected by the metal flow characteristics associated with the FSW process [25].

The microhardness value of Specimen 3 in TMAZ of the AS was measured at 56.52 HV, which was the lowest value. Also, the microhardness value of Specimen 3 in SZ was measured at 68.34 HV, which was

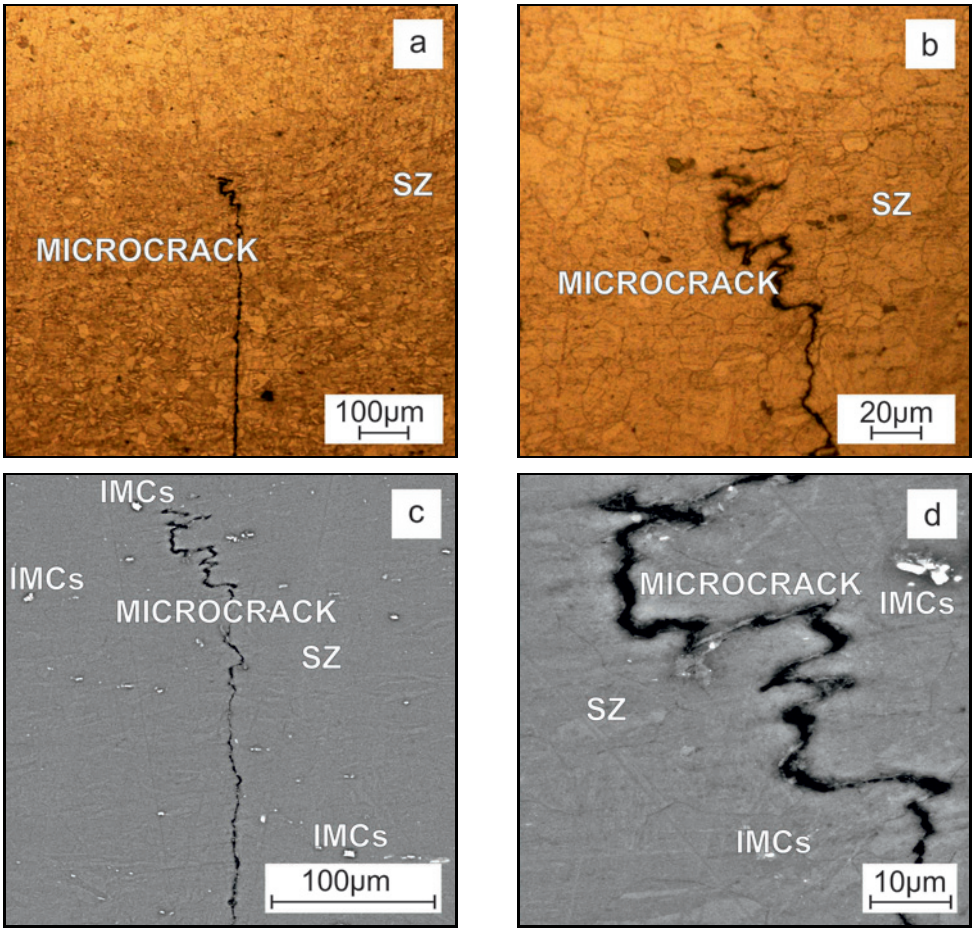

Fig. 6. OM images of (a), (b) microcrack in the SZ region and SEM images of (c), (d) IMCS and microcrack in the SZ region of Specimen 2.

Table 3. Content of elements at the points marked in Figs. 7 and 9a,b by EDX analysis (wt.%)

	Elements (wt.%)								
	C	O	Mg	Al	Si	Mn	Zn	Ca	Ce
Analysis number 1	12.05	12.64	23.62	23.96	–	27.57	0.16	–	–
Analysis number 2	3.81	19.67	66.32	1.84	7.00	0.96	0.40	–	–
Analysis number 3	12.21	15.78	28.54	18.40	0.61	24.20	–	0.25	–
Analysis number 4	6.40	4.05	33.46	25.58	–	30.27	0.24	–	–
Analysis number 5	6.22	4.04	68.26	0.73	20.45	–	0.31	–	–
Analysis number 6	6.02		13.94	47.69	–	29.69	–	–	–
Analysis number 7	6.00	3.37	63.33		27.30	–	–	–	–
Analysis number 8	6.74	3.33	22.30	42.89	–	24.76	–	–	–
Analysis number 9	9.80	5.35	64.62	12.22	–	4.04	0.68	–	3.30
Analysis number 10	13.19	16.18	20.67	14.92	–	34.84	–	0.21	–
Analysis number 11	4.27	2.76	39.42	28.40	–	14.39	–	–	10.76

the highest value. It is thought that the microhardness values changed with an increase in the hardness of the $Al_{12}Mg_{17}$ IMCs generated because of the heat input in the welding zone during the FSW of AZ31B Mg alloys. Previous studies support this [4, 14, 30, 31].

Figures 5a,b,c,e show OM images of the welding zone of Specimen 3. Figure 5d shows the SEM image of Specimen 3. Figure 5 shows AZ31B Mg sheets materials stirred fully with each other in the welding zone. It is seen that the fine-grained structure of the SZ has a homogeneous distribution. Rising the temperature and stirring impact of the pin raised the extrusion de-

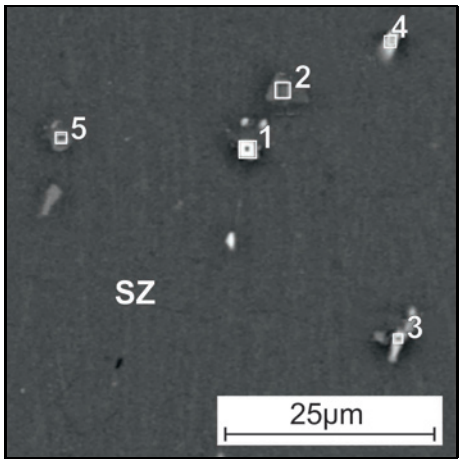

Fig. 7. SZ of Specimen 3.

gree in the material, which became viscous. Thus, in the SZ, a structure with grain shrinkage and hardening emerged. The deformation and extrusion severity generated during the FSW process and caused the grains to shrink in the SZ. In addition, bigger-sized coarse-grained structure stands out in TMAZ compared to the grain size in SZ [6, 17, 19, 30]. This can be attributed to the lower heat input to TMAZ and plastic deformation during the welding process. HAZ is shown in Figs. 5a,c,e. The weakest region of the welding zone is HAZ, which has the biggest grain size [6, 17, 19]. The HAZ corresponds to the weakest and least rigid area. Because HAZ is exposed to high temperatures, the precipitated particles continue to grow and display roughness. Therefore, the interval between the particles grows. Dislocations move easily in HAZ without colliding with any obstacles.

On the other hand, fractures and failures are found in HAZ, thereby reducing the strength. Welded specimens that were tensile tested were usually broken from this area [4, 14, 17, 20, 30]. Figure 5d shows that IMCs occurred in the welded zone of Specimen 3, which can be observed as white specks. According to the SEM images and OM images, Specimen 3 was successfully welded by FSW.

Figures 6a,b present the OM images of Specimen 2. Figures 6c,d show the SEM images of the welding zone of Specimen 2. Heat input is a significant parameter for FSW. It plays a significant role in the mechanical and microstructural properties of joints. Tool rotation speed and feed rate control the heat input in the welding area of joints during the FSW operation. High tool rotational speed with the unnecessary release of stirred material on the top surface leads to macroscopic defects, such as poor surface (flash), voids, tunneling, porosity, wormhole formation, and microcracks, due to the high heat input created by welding. From the results, it can be understood that the higher tool rotational speed created a higher amount of heat. Also, the higher amount of heat raised more thermal stresses directly during cooling. These stresses were unstable and led to defects during the cooling in the form of cracks [31]. At 1400 rpm with 50 mm min^{-1} feed rate, the amount of heat generated was higher and led to crack, as shown in Figs. 6a–d. Specimen 2 had the lowest welding strength because of the crack that occurred in the SZ [4, 14]. At 900 rpm with 50 mm min^{-1} feed rate, sufficient time was allowed to raise the temperature, and material plastic flow was sufficient to develop a perfect metallurgical joint which avoided the defect and resulted in a sound joint, as shown in Figs. 5a–e.

Figure 7 represents the SZ of Specimen 3. Figures 8a–e illustrate the results of the EDX analysis with numbers from 1 to 5 performed on the welding zone of Specimen 3. Table 3 shows the content of elements at the points marked in Figs. 7, 9a,b by EDX analysis (wt.%).

Figures 9a,b show the SZ of Specimen 2. Also, Figs. 10a–f and Table 3 demonstrate the results of the EDX analysis (wt.%) with analysis numbers from 6 to 11 performed on the welding zone of Specimen 2. According to the EDX analysis results, in addition to the increase of wt.% Al and wt.% O elements, there is also an increase in wt.% Mn and wt.% Si elements at some points. It is thought that the oxides at SZ can be the result of preexisting oxides or might have formed by the oxidation of Mg and alloying elements during FSW [25]. Increasing Al element volume and the existence of BM Mg element volume in the EDX analyses results of Specimens 2 and 3 support the presence of $Al_{12}Mg_{17}$ IMCs in the welding zone during the FSW process of Mg alloys. EDX analysis reveals that the SZ contains grains with significantly refined $Al_{12}Mg_{17}$ IMCs, which are homogeneously distributed in the magnesium matrix. During the FSW process, magnesium grains plastically deform with the effect of rotation of the tool. However, the second phase (brittle phase) is hard to deform. This causes stress concentration in the second phase. When the applied stress is higher than the fracture strength of the second phase, fracture occurs, and large second phases gradually change into smaller ones. The EDX analysis indicated that the IMCs in the stir zone were $Al_{12}Mg_{17}$ [6, 19, 30, 31].

4. Conclusions

In this study, AZ31B Mg alloy was successfully joined by FSW. Specimen 3 displayed the highest value of welding strength (176.03 MPa). Specimen 2 (50/0°/1400) showed the lowest welding strength (127.26 MPa) in the study.

When the tool rotation speed was increased from

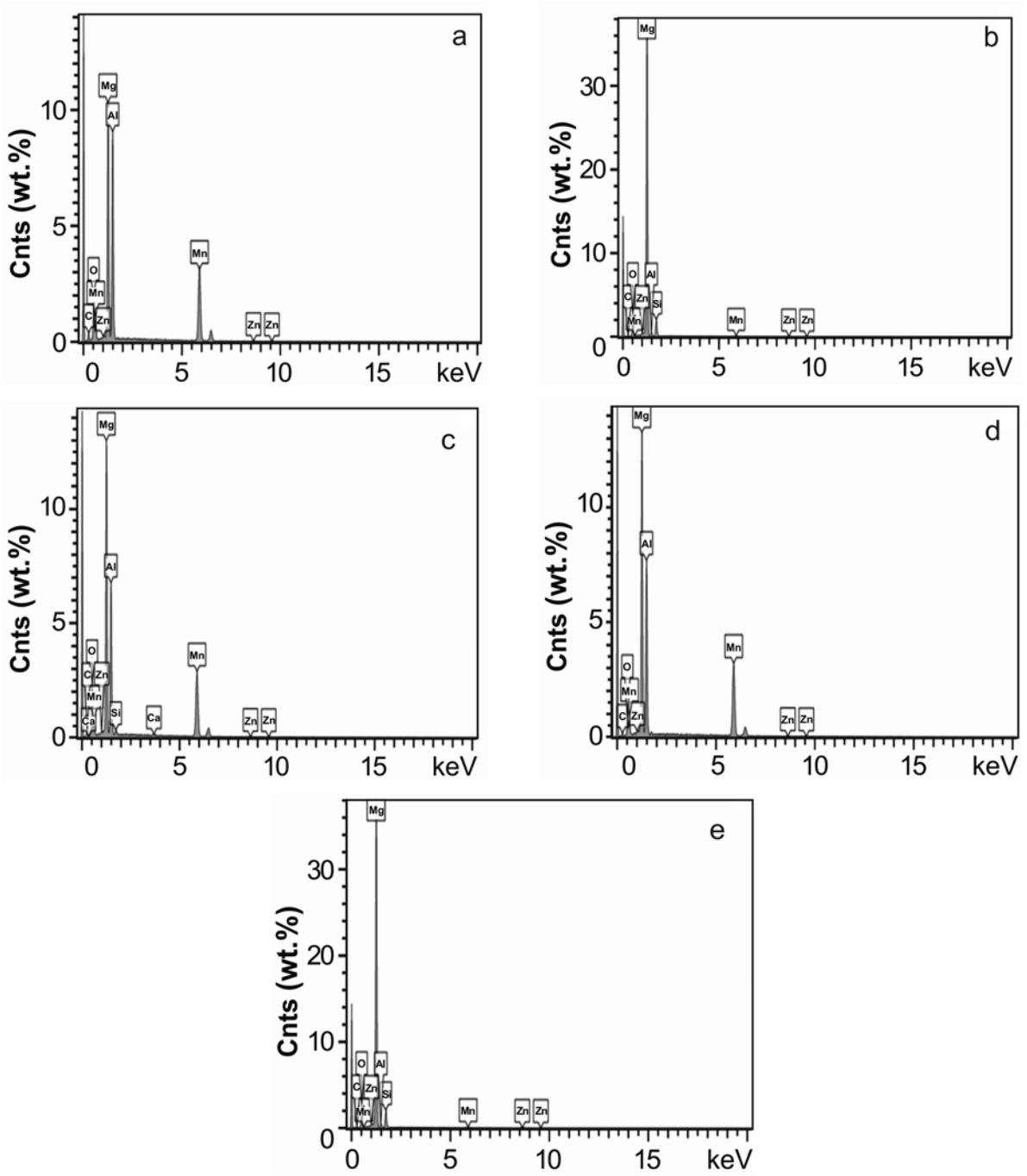

Fig. 8. EDX analysis number of (a) 1, (b) 2, (c) 3, (d) 4, and (e) 5 of SZ of Specimen 3.

900 to 1400 rpm, welding strength was decreased. During the joining of AZ31B Mg alloy by FSW, $Al_{12}Mg_{17}$ IMCs occur. Because the $Al_{12}Mg_{17}$ IMCs peaked at a high tool rotational speed of 1400 rpm, the welding strength of the specimens under a tool rotational speed of 1400 rpm was also decreased.

The study results demonstrate that the tool tilt angle had an essential effect on the mechanical properties of the welded specimens. The highest strength values of welded specimens were observed in the welding processes when a 1.5° tool tilt angle was used.

When the macro images of the specimens are examined, the weld seams of Specimens 1, 3, and 4 are smooth and even, while the weld seam of Specimen 2 is rough and uneven. A crack form is also remarkable in the OM, and SEM images of the weld region of Specimen 2 showed the lowest welding strength according to the tensile test results. It is thought that the rough and crack structure observed in the weld seam adversely affects the mechanical properties of the weld region.

The microhardness measurement graphs indicated

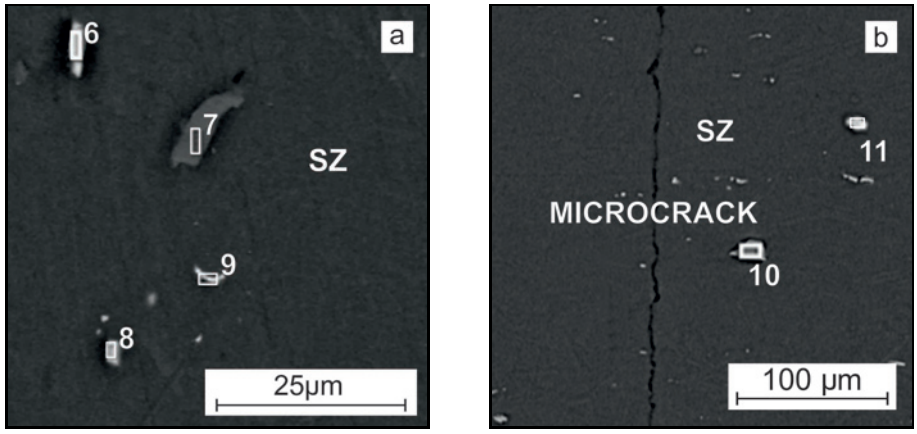

Fig. 9. (a), (b) SZ of Specimen 2.

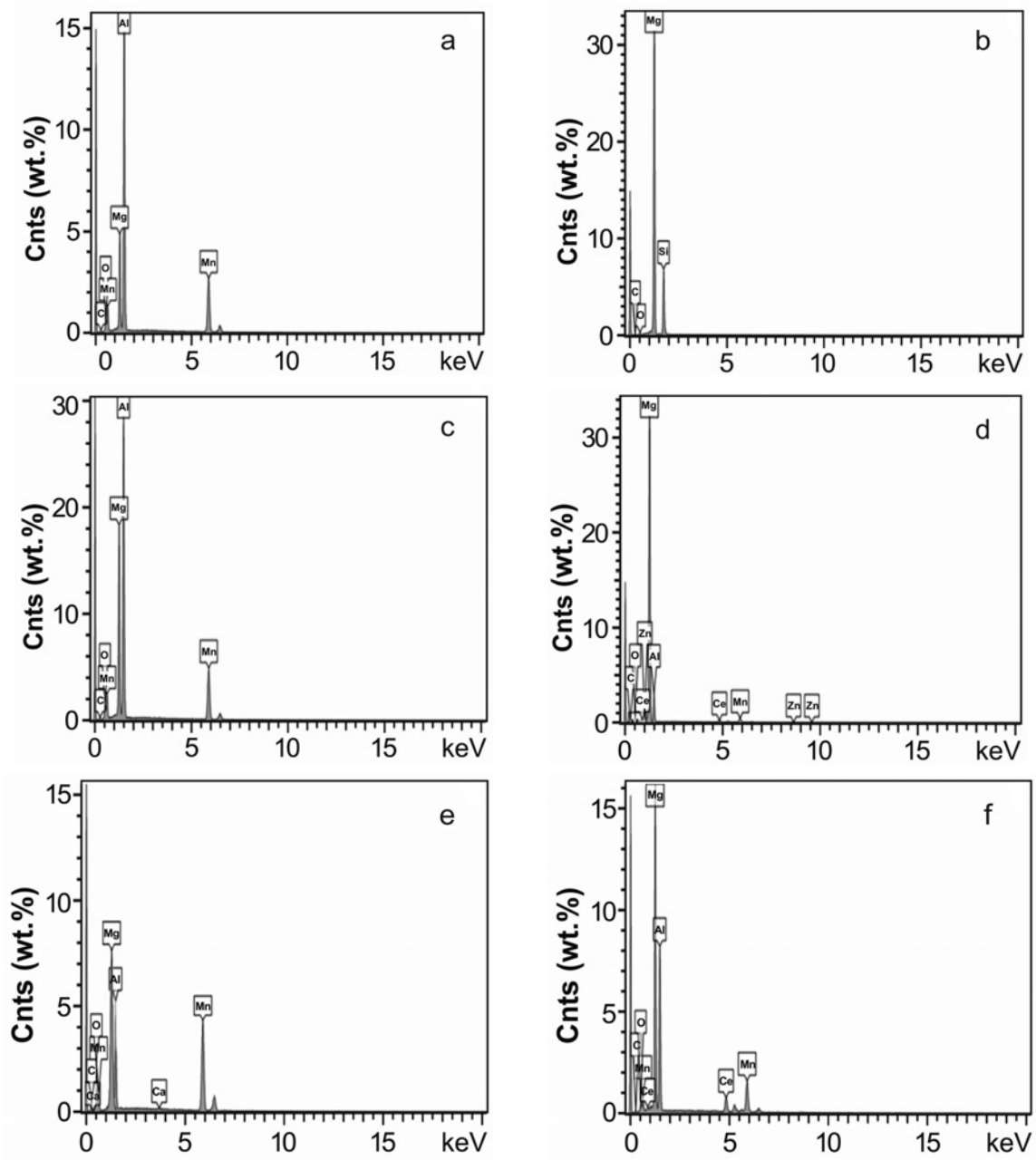

Fig. 10. EDX analysis number of (a) 6, (b) 7, (c) 8, (d) 9, (e) 10, and (f) 11 of SZ of Specimen 2.

that the hardness values of all the specimens were similar. It is seen that the microhardness values were increased in the SZ of specimens. All joints showed typical W-shaped microhardness profiles in the welding area. As it moves away from the welding center, values close to the microhardness value of the base material were measured. The microhardness decreased in the HAZ and TMAZ. Microhardness of Specimen 3 was measured at 68.35 HV in SZ. It is thought that the changed microhardness values with an increase in the hardness of the $Al_{12}Mg_{17}$ IMCs generated because of the heat input in the welding zone during the FSW of AZ31B Mg alloys. Also, the microhardness value of Specimen 3 in TMAZ of the AS was measured at 56.52 HV, which was the lowest value.

Finally, when the EDX analyses of Specimens 2 and 3 in SZ were examined, the density increase of the Al element supported the presence of $Al_{12}Mg_{17}$ IMCs in the weld zone. EDX analysis reveals that the mixing zone contains grains with significantly refined $Al_{12}Mg_{17}$ IMCs homogeneously dispersed in the magnesium matrix.

Acknowledgement

This study was supported by Balikesir University Scientific Research Project Unit (Project No: 2018/164).

References

[1] N.P. Papenberg, S. Gneiger, I. Weißensteiner, P. J. Uggowitzer, S. Pogatscher, Mg-alloys for forging applications – A review, Materials 13 (2020) 985. https://doi.org/10.3390/ma13040985

[2] F. Tolun, Application of Magnesium Alloys in Industry, 3th International Conference on Awareness, ICA2019 (2019), pp. 91–116. E-ISBN: 978-625-7047-00-5

[3] W. J. Joost, P. E. Krajewski, Towards magnesium alloys for high-volume automotive applications, Scripta Materialia 128 (2017) 107–112. https://doi.org/10.1016/j.scriptamat.2016.07.035

[4] S. Çelik, F. Tolun, Effect of double-sided friction stir welding on the mechanical and microstructural characteristics of AA5754 aluminium alloy, Materials Testing 63 (2021) 829–835. https://doi.org/10.1515/mt-2021-0009

[5] H. H. Jadav, V. Badheka, D. K. Sharma, G. Upadhyay, A review on effect of friction stir processing on the welded joints, Materials Today: Proceedings 43 (2021) 84–92. https://doi.org/10.1016/j.matpr.2020.11.215

[6] G. Padmanaba, V. Balasubramanian, An experimental investigation on friction stir welding of AZ31B magnesium alloy, International Journal of Advanced Manufacturing Technology 49 (2010) 111–121. https://doi.org/10.1007/s00170-009-2368-1

[7] A. Azizi, H. Alimardan, Effect of welding temperature and duration on properties of 7075 Al to AZ31B Mg diffusion bonded joint, Transaction Nonferrous Metals Society of China 26 (2016) 85–92. https://doi:10.1016/S1003-6326(16)64091-8

[8] K. Hao, H. Wang, M. Gao, R. Wua, X. Zeng, Laser welding of AZ31B magnesium alloy with beam oscillation, Journal of Materials Research and Technology 8 (2019) 3044–3053. https://doi.org/10.1016/j.jmrt.2019.04.024

[9] C. Li, L. Liu, Investigation on weldability of magnesium alloy thin sheet T-joints: Arc welding, laser welding, and laser-arc hybrid welding, International Journal of Advanced Manufacturing Technology 65 (2013) 27–34. https://doi.org/10.1007/S00170-012-4145-9

[10] G. Liang, S. Yuan, Study on the temperature measurement of AZ31B magnesium alloy in gas tungsten arc welding, Materials Letters 62 (2008) 2282–2284. https://doi.org/10.1016/j.matlet.2007.11.096

[11] L. Liu, G. Song, G. Liang, J. Wang, Pore formation during hybrid laser-tungsten inert gas arc welding of magnesium alloy AZ31B – mechanism and remedy, Materials Science and Engineering A 390 (2005) 76–80. https://doi.org/10.1016/j.msea.2004.07.067

[12] Z. Zhang, X. Kong, Study on DC double pulse metal inert gas (MIG) welding of magnesium alloy, Materials and Manufacturing Processes 27 (2012) 462–466. https://doi.org/10.1080/10426914.2011.585500

[13] Y. Luo, G. You, H. Ye, J. Liu, Simulation on welding thermal effect of AZ61 magnesium alloy based on three-dimensional modeling of vacuum electron beam welding heat source, Vacuum 84 (2010) 890–895. https://doi.org/10.1016/j.vacuum.2009.12.005

[14] F. Tolun, Mechanical and microstructural properties of friction stir welded AA5083 and AA5754 aluminium alloys, Kovove Mater. 59 (2021) 149–160. https://doi.org/10.4149/km_2021_3_149

[15] F. Tolun, Recent advanced welding techniques for magnesium alloys, Journal of Current Research on Engineering, Science and Technology 6 (2020) 49–60.

[16] S. K. Dewangan, M. K. Tripathi, M. K. Manoj, Material flow behavior and mechanical properties of dissimilar friction stir welded al 7075 and Mg AZ31 alloys using Cd interlayer, Metals and Materials International (2021). https://doi.org/10.1007/s12540-021-00980-1

[17] A. Thakur, V. Sharma, S. S. Bhadauria, Effect of tool tilt angle on weld joint strength and microstructural characterization of double-sided friction stir welding of AZ31B magnesium alloy, CIRP Journal of Manufacturing Science and Technology 25 (2021) 132–145. https://doi.org/10.1016/j.cirpj.2021.05.009

[18] J. Zhang, Y. Huang, J. Xiang, G. Huang, X. Chen, H. Zhou, B. Jiang, A. Tang, F. Pan, Characterization of newly developed friction stir-arc welding method for AM60/AZ31 dissimilar Mg alloy, Materials Science and Engineering A 800 (2021) 140320. https://doi.org/10.1016/j.msea.2020.140320

[19] M. Sucharitha, B. Ravi Sanka, P. Umamaheswarrao, Experimental investigations on the effect of tool rotational speed on mechanical properties and microstructure of friction stir welded AZ31 Mg alloy, Materials Today: Proceedings 46 (2020) 3455–3459. http://dx.doi.org/10.1016/j.matpr.2020.11.788

[20] W. Lia, P. L Niua, S. R. Yana, Vivek Patela, Q. Wen, Improving microstructural and tensile properties of AZ31B magnesium alloy joints by stationary shoulder

friction stir welding, Journal of Manufacturing Processes 37 (2019) 159–167. https://doi.org/10.1016/j.jmapro.2018.11.014

[21] P. Kumar, L. Thakur, N. Bhadouria, S. Dixit, Microstructure and mechanical behaviour of friction stir processed AZ91-D magnesium alloy – optimization of process parameters by using the Taguchi method, Kovove Mater. 57(2019) 207–217. https://doi.org/10.4149/km_2019_3_207

[22] N. Xu, Q. Song, H. Fujii, Y. Bao, J. Shen, Mechanical properties' modification of large load friction stir welded AZ31B Mg alloy joint, Materials Letters 219 (2018) 93–96. https://doi.org/10.1016/j.matlet.2018.02.099

[23] S. Mironova, T. Onumaa, Y. S. Satoa, S. Yoneyamab, H. Kokawaa, Tensile behavior of friction-stir welded AZ31 magnesium alloy, Materials Science and Engineering A 679 (2017) 272–281. https://doi.org/10.1016/j.msea.2016.10.036

[24] H. Shi, K. Chen, Z. Liang, F. Dong, T. Yu, X. Dong, L. Zhang, A. Shan, Intermetallic compounds in the banded structure and their effect on mechanical properties of Al/Mg dissimilar friction stir welding joints, Journal of Materials Science and Technology 33 (2017) 359–366. https://doi.org/10.1016/j.jmst.2016.05.006

[25] M. Pareek, A. Polar, F. Rumiche, J. E. Indacochea, Metallurgical evaluation of AZ31B-H24 magnesium alloy friction stir welds, Journal of Materials Engineering and Performance 16 (2007) 655–662. https://doi.org/10.1007/s11665-007-9084-5

[26] ASTM E8-04, Standard Test Methods for Tension Testing of Metallic Materials, West Conshohocken, ASTM International 2020.

[27] M. M. Z. Ahmed, S. Ataya, M. M. El-Sayed Seleman, A. M. A. Mahdy, N. A. Alsaleh, E. Ahmed, Heat input and mechanical properties investigation of friction stir welded AA5083/AA5754 and AA5083/AA7020, Metals 11 (2021) 68. https://doi.org/10.3390/met11010068

[28] V. Patel, W. Li, G. Wang, F. Wang, A. Vairis, P. Niu, Friction stir welding of dissimilar aluminum alloy combinations: State-of-the-art, Metals 9 (2019) 270. http://doi:10.3390/met9030270

[29] A. Tongne, C. Desrayaud, M. Jahazi, E. Feulvarch, On material flow in friction stir welded Al alloys, Journal of Materials Processing Technology 239 (2017) 284–296. https://doi.org/10.1016/j.jmatprotec.2016.08.030

[30] A. M. Desai, B. C. Khatri, V. Patel, H. Rana, Friction stir welding of AZ31 magnesium alloy: A review, Materials Today: Proceedings 47 (2021) 6576–6584. https://doi.org/10.1016/j.matpr.2021.03.082

[31] B. R. Sunil, G. P. K. Reddy, A. S. N. Mounika, P. N. Sree, P. R. Pinneswari, I. Ambica, R. A. Babu, P. Amarnadh, Joining of AZ31 and AZ91 Mg alloys by friction stir welding, Journal of Magnesium and Alloys 3 (2015) 330–334. https://doi.org/10.1016/j.jma.2015.10.002